Journal of Power Sources 247 (2014) 497–502

Contents lists available at ScienceDirect

Journal of Power Sources

journal homepage: www.elsevier.com/locate/jpowsour

Short communication

Lithium deficient mesoporous $Li_{2-x}MnSiO_4$ with significantly improved electrochemical performance

Haiyan Wang [a, *], Tianli Hou [a], Dan Sun [a], Xiaobing Huang [b], Hanna He [a], Yougen Tang [a], Younian Liu [a]

[a] School of Chemistry and Chemical Engineering, Central South University, Changsha 410083, PR China
[b] College of Chemistry and Chemical Engineering, Hunan University of Arts and Science, Changde 415000, PR China

HIGHLIGHTS

- Lithium deficient mesoporous $Li_{2-x}MnSiO_4$ compounds are first proposed.
- $Li_{2-x}MnSiO_4$ compounds exhibit improved electrochemical performance.
- $Li_{1.8}MnSiO_4$ delivers a discharge capacity of 110.9 mAh g^{-1}, with 90.8 mAh g^{-1} remaining after 25 cycles.
- The superior properties are due to the improvement of electronic conductivity and structure stability.

ARTICLE INFO

Article history:
Received 30 July 2013
Received in revised form
23 August 2013
Accepted 26 August 2013
Available online 4 September 2013

Keywords:
Li-ion batteries
Lithium manganese silicate
Lithium deficient chemistry
Mesoporous structure
Electrochemical performance

ABSTRACT

$Li_{2-x}MnSiO_4$ compounds with mesoporous structure are first proposed in the present work. It is interesting to note that the lithium deficient compounds exhibit much higher electrochemical performance in comparison with the stoichiometric one. Among these compounds, $Li_{1.8}MnSiO_4$ shows the best electrochemical performance. It is found that mesoporous $Li_{1.8}MnSiO_4$ without carbon coating delivers a maximum discharge capacity of 110.9 mAh g^{-1} at 15 mA g^{-1}, maintaining 90.8 mAh g^{-1} after 25 cycles, while that of the stoichiometric one is only 48.0 mAh g^{-1}, with 12.5 mAh g^{-1} remaining. The superior properties are mainly due to the great improvement of electronic conductivity and structure stability, as well as suppressed charge-transfer resistance.

1. Introduction

The orthosilicate family of Li_2MSiO_4, where M is some transition-metals Fe, Mn or Co, are highlighted as interesting candidates for lithium battery cathodes by virtues of their potential ability to facilitate the extraction of more than one Li ions per transition metal, low cost and high safety [1–5]. Two Li ions could be theoretically extracted from Li_2MnSiO_4, giving the theoretical capacity of 333 mAh g^{-1}. Therefore, Li_2MnSiO_4, as a new cathode material, has attracted a great deal of attentions. There are not too many reports involving the electrochemical characterizations of Li_2MnSiO_4 because of their poor electronic conductivity and tendency to become the amorphous after the extraction of Li ions [6–11]. It is reported that its electronic conductivity is even less than 10^{-14} S cm^{-1} at room temperature, which makes the electrode material be almost electrochemical inactive [2]. Li et al. [9] prepared the carbon coated Li_2MnSiO_4, which showed a high initial discharge capacity of 209 mAh g^{-1}. However, the as-prepared Li_2MnSiO_4 without carbon only delivered a very low discharge capacity of 10 mAh g^{-1}. Dominko et al. [12] found that only 0.6 Li could be inserted into Li_2MnSiO_4 in the initial cycle. At the 5th cycle, only 0.3 Li could be reversible exchanged.

Much work has devoted to the structure analysis [13–15]. And some novel preparation methods have been developed in recent years for Li_2MnSiO_4 [16]. High reversible capacity of more than 300 mAh g^{-1} at elevated temperature has been achieved [17]. Partial Fe replacing Mn [18] and Cr-doping [19] have been considered good ways to stabilize the crystal. However, it is still a big challenge to address the structural instability in essence.

* Corresponding author. Tel.: +86 0731 8830886; fax: +86 0731 8879616.
E-mail address: wanghy419@126.com (H. Wang).

0378-7753/$ – see front matter © 2013 Elsevier B.V. All rights reserved.
http://dx.doi.org/10.1016/j.jpowsour.2013.08.115

Therefore, a novel strategy should be explored to further enhance its electrochemical properties. Defect chemistry is considered as a very powerful approach to better the electronic conductivity of the electrode materials, thus resulting in high performance. In our previous work, $Li_{1.95}FeSiO_4$/C composite with improved rate capability was synthesized [20]. Herein, $Li_{2-x}MnSiO_4$ with higher reversible capacity and superior cycling stability is proposed, which will open up a new direction for achieving the high performance of silicates and other electrode materials for Li-ion battery.

2. Experimental

2.1. Synthesis

Starting materials with analytical pure grade are used directly without any purification. A stoichiometric amount (the molar ratio of Li:Mn:Si is 2:1:1) of lithium acetate dehydrate ($LiAC\cdot 2H_2O$), manganese acetate tetrahydrate ($MnAC_2\cdot 4H_2O$) and $Si(OC_2H_5)_4$ (TEOS) were dissolved in ethanol and distilled water mixed solution (Ve/Vw = 4:1). The mixed solution was stirred at 90 °C for 8 h using a reflux cooling system. Then the reflux cooling system was removed and the mixed solution containing the hydrolyzed SiO_2 from TEOS was evaporated at 95 °C to form the wet gel. As follows, the wet gel was dried at 80 °C overnight in the drying oven and the resulting precursor was finely ground by agate mortar and then pressed into pellets and calcined at 700 °C for 10 h in a flow of Ar. $Li_{2-x}MnSiO_4$ compounds ($x = 0.1$, 0.2, 0.3) were prepared with the similar procedure above only adjusting the amount of $LiAC\cdot 2H_2O$.

2.2. Characterization

X-ray diffraction (XRD) data of as-prepared powder and the electrodes after cycling with different voltages were collected by a Dandong Haoyuan X-ray diffractometer (DX-2700) utilizing a Cu-Kα1 source. Morphological studies were conducted using a JEOL JEM-2100F transmission electron microscopy (TEM) with an accelerating voltage of 200 keV. N_2 adsorption–desorption analysis was carried out using a Builder SSA-4200 at −196 °C. The element analysis of $Li_{1.8}MnSiO_4$ was carried out by a Pye Unicam SP2900 atomic-absorption spectrophotometer (AAS) and the exact lithium coefficient in $Li_{1.8}MnSiO_4$ is determined to be 1.788, slight difference with the theoretical one.

2.3. Electrochemical measurements

Cathodes for electrochemical measurement were constructed by mixing the active material, polyvinylidene fluoride (PVDF), and Super S carbon in the weight ratio of 80:10:10. *N*-methyl pyrrolidone was used as solvent. The slurry was cast onto Al foil using the Doctor-Blade technique. After solvent evaporation at 100 °C under vacuum for 8 h, the electrodes were assembled into coin-type cells with a lithium metal disk as counter electrode and commercial electrolyte (Guangzhou Tinci; 1 M $LiPF_6$ in 1:1 v/v ethylene carbonate/dimethyl carbonate). The loading mass of each electrode ranges from 1.5 to 2.5 mg cm^{-2}. The assembled electrochemical cell was tested between 1.5 and 4.8 V (versus Li^+/Li) at a desired current density with a Neware battery testing system (CT-3008W) at room temperature. Electrochemical impedance spectroscopy (EIS) was recorded at 2.9 V by a Princeton workstation (PARSTAT2273, EG&G, US) over the frequency range from 500 kHz to 10 mHz with an amplitude of 5 mV.

3. Results and discussion

XRD patterns (Fig. 1) reveal that all as-prepared compounds match Li_2MnSiO_4 (orthorhombic structure, space group $Pmn2_1$) phase well, which is analogous to Li_3PO_4 [9]. Note that all $Li_{2-x}MnSiO_4$ materials exhibit the low level impurity of MnO (2θ = 34.9°, 40.6°) and the lithium deficient compounds show the new impurity of Mn_2SiO_4 (2θ = 34.9°, 40.6°). The diffraction lines of Mn_2SiO_4 increase with the increasing of lithium deficient content. Factually, it was difficult to obtain an impurity-free Li_2MnSiO_4 since the overlap existed between the stability domains of the main and impurity phase [21,22]. In addition, the intensity of the main diffraction patterns decreases gradually with the increasing amount of the deficient lithium, implying the inferior crystalline. Bragg peaks are somewhat broadened, suggesting the presence of small crystalline particles. The average crystalline size of 3.78 nm could be calculated for $Li_{1.8}MnSiO_4$ according to the Scherrer's equation, which is close to the following HRTEM results (6–8 nm, Fig. 2d and e). The lattice parameters of Li_2MnSiO_4 are a = 0.6288 nm, b = 0. 5362 nm, c = 0. 4983 nm, consistent with values published by others [9]. Based on the calculated lattice parameters (Table 1), it is found that lithium deficient compounds demonstrate the expanding a and b axis, as well as contracting c axis, thus resulting in somewhat increased crystal volume.

The sample features a uniform primary particle size distribution of 6–8 nm, as clearly revealed by the TEM images (Fig. 2a–e), which basically agrees the calculated results from the Scherrer's equation. Interestingly, the particles are aggregated to form the honeycomb-like morphology, some of which are of aqusi-sphere with the average diameter of *ca.* 80 nm. To the best of our knowledge, no paper involved such morphology for Li_2MSiO_4 (M = Mn, Fe). The formation of mesoporosity may be in part due to the decomposition of the raw materials at high temperature accompanying with the release of CO_2 and H_2O. The mesostructure of as-prepared product are further demonstrated by HRTEM images (Fig. 2d and e), which will provide enough spaces for contacting of electrolyte and active materials. Interestingly, a number of amorphous domains are observed in the particles (highlighted by red lines in the web version), leading to the observed discontinuity of the crystal lattices. The clear lattice spacing on the edge of particles provides the absent evidence of residual carbon coating. In addition, high

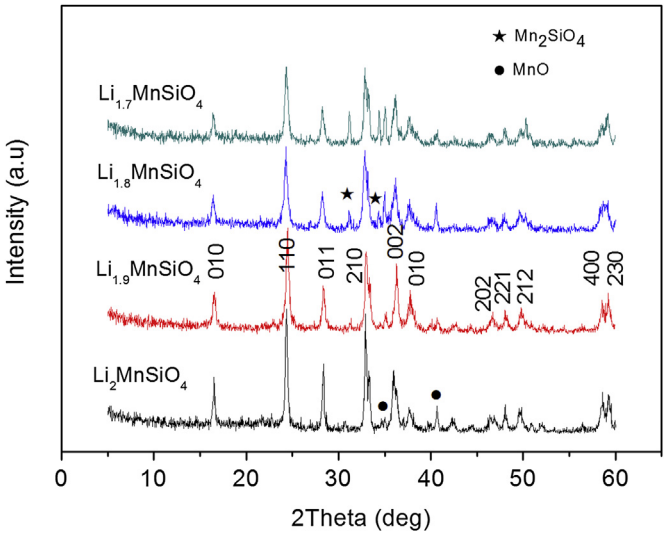

Fig. 1. XRD patterns of as-prepared $Li_{2-x}MnSiO_4$ (x = 0, 0.1, 0.2, 0.3).

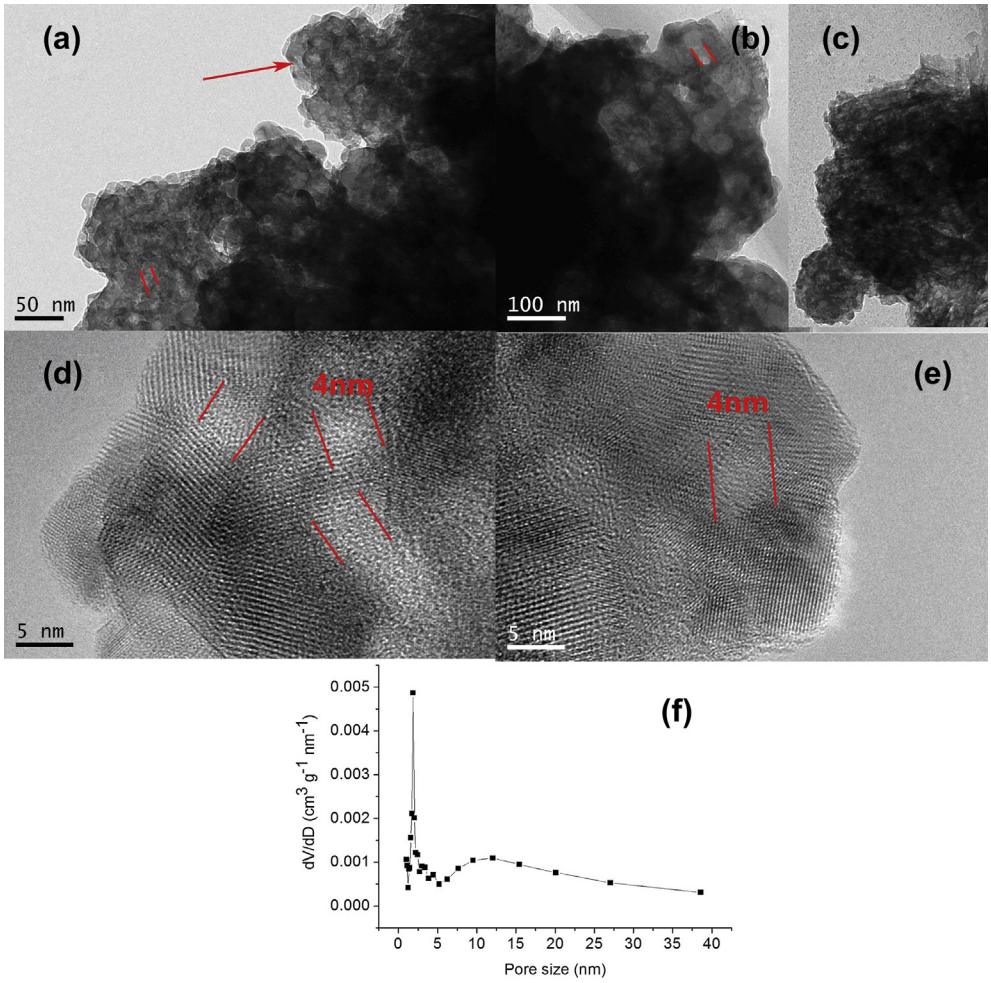

Fig. 2. TEM (a, b, c) and HRTEM (d, e) images of as-prepared $Li_{1.8}MnSiO_4$, associated with the pore size distributions (f) from the desorption curve.

crystallization is also observed, which would benefit its electrochemical performance.

The mesostructure was further supported by the nitrogen adsorption–desorption measurement. The Brunauer–Emmett–Teller (BET) surface area for $Li_{1.8}MnSiO_4$ is *ca.* 34 $m^2\ g^{-1}$. The corresponding pore size distributions, calculated from desorption isotherms, is given in Fig. 2f. It exhibits a narrow distribution centred at ~2 nm and a broad distribution peaked at ~10 nm, consistent with the mesoporosity observed by HRTEM images (Fig. 2d and e).

Galvanostatic charge/discharge cycling test (Fig. 3a) at 15 mA g^{-1} was performed. As shown, Li_2MnSiO_4 delivers an initial discharge capacity of 67.5 mAh g^{-1}, corresponding to the insertion of 0.41 Li. It was reported that electronic conductivity of Li_2MSiO_4 is extremely low, which is even up to 3 orders of magnitude lower than that of $LiFePO_4$, thus resulting in pure-phase Li_2MSiO_4 electrochemically inactive [2,12]. Li_2MnSiO_4 without carbon coating by Yang et al. [9] exhibited a very low discharge capacity of 10 mAh g^{-1}. Dominko et al. [12] found that only 0.3 Li could be reversible exchanged at the 5th cycle. In this work, large capacity loss is found in the following cycles, only 12.5 mAh g^{-1} remaining at the 25th cycle, consistent well with the results in literature [9,12]. It is worthwhile to note that lithium deficient materials show improved electrochemical performance. The initial discharge capacity of $Li_{1.9}MnSiO_4$ is increased to 109.3 mAh g^{-1} and about 60 mAh g^{-1} is retained after 25 cycles. Although the discharge capacity of the first two cycles for $Li_{1.8}MnSiO_4$ is a little low, it is gradually increased to 110.9 mAh g^{-1} at the 4th cycle and then keeps stable in the first 13 cycles. After an obvious capacity fading in the following several cycles, the electrode shows the capacity of 96.0 mAh g^{-1}. As follows, no considerable capacity loss is observed. Results above indicate the superior cycling stability for $Li_{1.8}MnSiO_4$ with the capacity retention of *ca.* 83.3% (based on the 3rd cycle). Note that more lithium deficiency in $Li_{1.7}MnSiO_4$ is unfavorable for further electrochemical performance improvement probably due to the appearance of more impurities. Fig. 3b presents the whole charge–discharge curves for $Li_{1.8}MnSiO_4$. As can be seen, the charge curves in the first two cycles are different, implying that electrode undergoes a slight structure arrangement. After that, the load curves demonstrate no considerable change. Rate performance of $Li_{1.8}MnSiO_4$ is also investigated (Fig. 3c). It exhibits a high discharge capacity of 147.1 mAh g^{-1} at 10 mA g^{-1}, corresponding to near 0.89

Table 1
The calculated lattice parameters of $Li_{2-x}MnSiO_4$ ($x = 0, 0.1, 0.2, 0.3$).

Samples	*a* (nm)	*b* (nm)	*c* (nm)	*V* (nm^3)
Li_2MnSiO_4	0.6288	0.5362	0.4983	0.1680
$Li_{1.9}MnSiO_4$	0.6289	0.5383	0.4965	0.1681
$Li_{1.8}MnSiO_4$	0.6301	0.5401	0.4959	0.1687
$Li_{1.7}MnSiO_4$	0.6313	0.5392	0.4959	0.1688

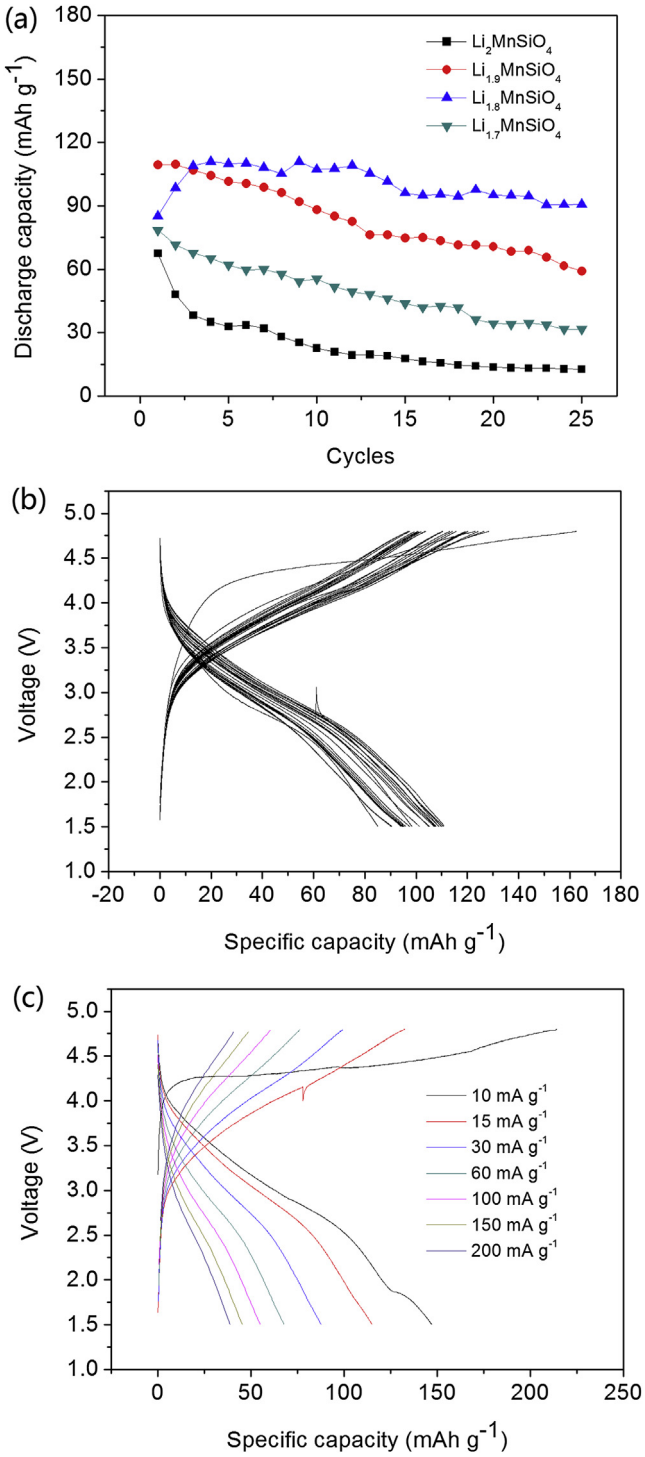

Fig. 3. (a) Cycling performance of $Li_{2-x}MnSiO_4$ ($x = 0, 0.1, 0.2, 0.3$) at 15 mA g^{-1}; (b) the corresponding load curves (25 cycles) of $Li_{1.8}MnSiO_4$; (c) the load curves of $Li_{1.8}MnSiO_4$ at various current densities from 10 mA g^{-1}–200 mA g^{-1}.

reversible Li ions. At 30 and 150 mA g^{-1}, it decreases to 87.6 and 45.9 mAh g^{-1}, respectively. Apparently, this is a high value for Li_xMnSiO_4 without carbon coating. Fig. 4 shows the initial charge–discharge curves of Li_2MnSiO_4 and $Li_{1.8}MnSiO_4$ at 15 mA g^{-1}. As can be seen, Li_2MnSiO_4 exhibits a large charge capacity of 251.8 mAh g^{-1} with a very low Coulombic efficiency (26.8%), as well as relatively high charge plateau (*ca.* 4.6 V). Note that the initial charge capacity of $Li_{1.8}MnSiO_4$ is decreased to 162.8 mAh g^{-1}

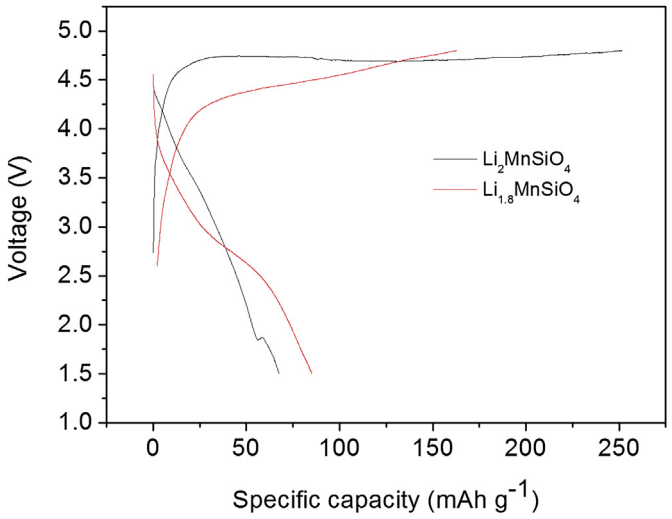

Fig. 4. The initial charge–discharge curves of Li_2MnSiO_4 and $Li_{1.8}MnSiO_4$ at 15 mA g^{-1}.

probably due to the deficient lithium ions in host, however, its initial Coulombic efficiency is increased to 52.1%. In addition, the difference of charge plateaus also demonstrates the effect of lithium deficiency to the crystal structure of Li_2MnSiO_4. Carbon coating or modification with other conductive agents is considered as promising way to better the electrochemical performance for those electrode materials with relatively low electronic conductivity [23,24]. Studies of carbon-coated lithium deficiency $Li_{2-x}MnSiO_4$ and its further improvement reasons are underway and will be given in our forthcoming article.

The electronic conductivity and electrochemical impedance spectroscopy (EIS) measurements were further employed to understand the intrinsic origins for the improved electrochemical performance of lithium deficient compounds. The electronic conductivity of $Li_{1.8}MnSiO_4$ by the four-point probe method (Suzhou Tongchuang, SZT-2B) was measured to be 8.2×10^{-6} S m^{-1}, which is about 5 orders of magnitude higher than that of Li_2MnSiO_4 (*ca.* 10^{-11} S m^{-1}). The electronic conductivity of Li_2MnSiO_4 is higher than that in Ref. [12] probably due to the unique morphology. It implies that the transferring of electron is greatly improved due to the existence of lithium deficient in as-prepared compounds. Similar results could be found for lithium deficient Li_xFePO_4 [25]. The Nyquist plots (Fig. 5a) demonstrate a semicircle in the high-medium frequency range and a slop line in the low frequency range. The data were analyzed by using the equivalent circuit model, the inset in Fig. 5a. In this model, R_e represents the ohmic resistance including total resistance of the electrolyte, separator, and electrical contacts. R_{ct} is the charge-transfer resistance and CPE1 is the constant phase angle element involving double layer capacitance. W_o (Warburg impedance) reflects the solid-state diffusion of Li^+ in the bulk of the active material [26–28]. Table 2 shows the impendence fitting results of Li_2MnSiO_4 and $Li_{1.8}MnSiO_4$ electrodes. As seen, except the R_e value, Li_2MnSiO_4 shows much larger R_{ct} (1340 Ω) and W_o impedance (401 Ω) because of its low conductivity. Apparently, R_{ct} impedance (138 Ω) of $Li_{1.8}MnSiO_4$ is greatly suppressed due to the introduction of Li deficiency.

It is well known that cycling stability of the electrode is greatly related to the retention of the crystal structure during the lithium ion insertion/extraction processes. According to the ex-situ XRD studies, Li et al. [9] revealed that severe crystal structure destruction of Li_2MnSiO_4 into amorphous phase appears during the cycling process, which was considered to be the main reason for large capacity loss. However, in our case, Li deficiency strategy for

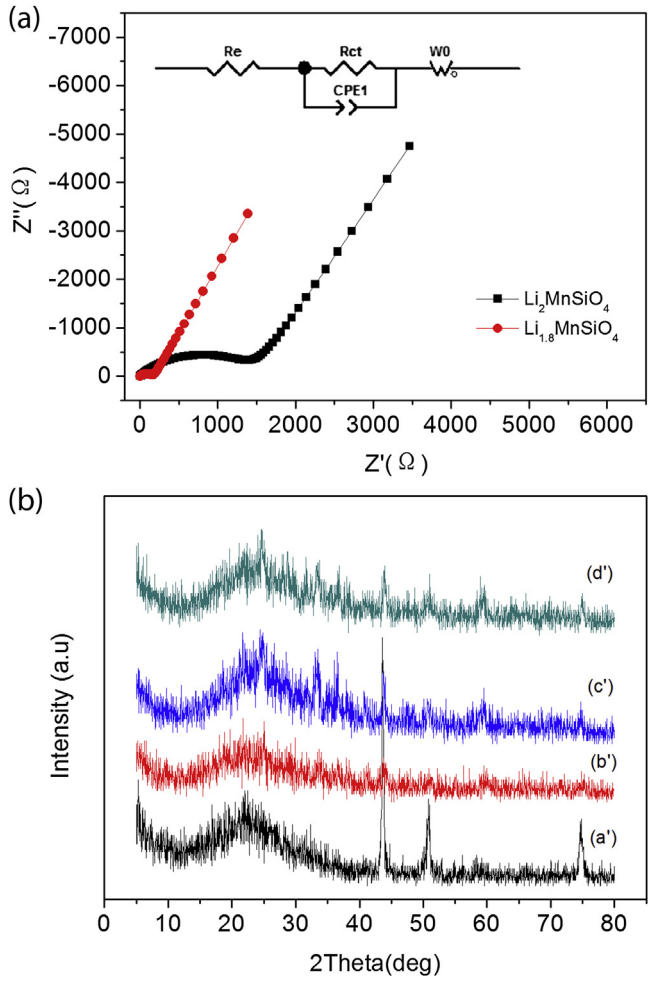

Fig. 5. (a) Nyquist plots of Li_2MnSiO_4 and $Li_{1.8}MnSiO_4$ electrodes at 2.9 V after 1 cycle at 15 mA g^{-1}, the inset in Fig. 4(a) is the equivalent circuit model used for the fitting; (b) XRD patterns of electrode under different states: a′-charge to 4.2 V, b′-charge to 4.8 V, c′ -charge to 3.0 V after one cycle, d′-charge to 3.0 V after 5 cycles.

$Li_{2-x}MnSiO_4$ enables much improved cycling stability and reversible capacity via enhancing the electronic conductivity and retaining the crystal structure. Fig. 5b shows the XRD patterns of $Li_{1.8}MnSiO_4$ at different states in the first several cycles. It should be pointed out that the construction of electrodes for XRD test is different from that for electrochemical measurement since the powder in electrode with Al foil as current collector after cycling tends to exfoliate when disassembling the cell. For address such issue, test electrodes were fabricated by pressing a mixture of active material, Super S carbon, and polytetrafluoro-ethylene (PTFE) in a weight ratio of 80:10:10 on a stainless steel mesh current collector at 20 MPa firstly and then dried at 110 °C for 8 h. As seen, XRD result of electrode is much different from as-prepared powder and the pattern lines vary with the extraction of Li ions from the host (electrode a′ and b′). Electrode c′ and d′ are cycled one and five cycles, respectively, and then both are recharged to 3.8 V. It is interesting to note that electrode after five cycles still maintains good crystal structure, rather than the amorphous phase. There is no obvious difference in XRD patterns of Electrode c′ and d′, suggesting that the lithium deficient compound possesses good structure stability during the cycling.

Table 2
The impendence fitting results of Li_2MnSiO_4 and $Li_{1.8}MnSiO_4$ electrodes at 2.9 V after 1 cycle at 15 mA g^{-1}.

Samples	R_e (Ω)	R_{ct} (Ω)	CPE1 (F)	CPE-*n*	W_o (Ω)
Li_2MnSiO_4	3.3	1340	1.47E-5	0.663	401
$Li_{1.8}MnSiO_4$	3.1	138	1.36E-4	0.69	118

Based on the above results, it is certain that the improvement of electrochemical properties for $Li_{1.8}MnSiO_4$ could be attributed to the introduction of appropriate Li deficiency strategy, which probably leads to the following reinforced effects: (1) crystal defect concentration is expected to be increased because of insufficient lithium source during the calcination, resulting in the significant enhancement of electronic conductivity; (2) Li deficiency compound shows the different interface electrochemical properties and the charge transfer process is greatly accelerated; (3) the structure instability into amorphous phase is well restricted, which provides an interesting approach to address the Li_2MnSiO_4's big issue.

4. Conclusions

In summary, lithium deficient strategy was proposed for the first time to improve the electrochemical performance of Li_2MnSiO_4 essentially. Mesoporous $Li_{1.8}MnSiO_4$ shows the best properties. It delivers a high discharge capacity of 147.1 mAh g^{-1} at 10 mA g^{-1}. The capacity retention of *ca.* 83.3% is achieved at 15 mA g^{-1} in the first 25 cycles. The electrochemical performance is significantly enhanced by virtue of lithium deficiency designing, which is beneficial for the improvement of electronic conductivity and structure stability, as well as suppressing charge-transfer resistance. This strategy could pave a new way for silicates and other polyanion-based compounds to achieve the significant improvement of electrochemical properties.

Acknowledgments

This project was financially supported by the National Nature Science Foundation of China (No. 21301193), China Postdoctoral Science Foundation Funded Project (No. 2013M530356), Fundamental Research Funds for the Central Universities of Central South University, Scientific Research Foundation of Key Laboratory of Resources Chemistry of Nonferrous Metals of Ministry of Education (No. 2012KF01) and the Open-End Fund for Valuable and Precision Instruments of Central South University (CSUZC201303).

References

[1] A. Nyten, A. Abouimrane, M. Armand, T. Gustafsson, J.O. Thomas, Electrochem. Commun. 7 (2005) 156–160.
[2] R. Dominko, M. Bele, A. Kokalj, M. Gaberscek, J. Jamnik, J. Power Sources 174 (2007) 457–461.
[3] Z. Gong, Y. Yang, Energy Environ. Sci. 4 (2011) 3223–3242.
[4] D.M. Kempaiah, D. Rangappa, I. Honma, Chem. Commun. 48 (2012) 2698–2700.
[5] A. Kokalj, R. Dominko, G. Mali, A. Meden, M. Gaberscek, J. Jamnik, Chem. Mater. 19 (2007) 3633–3640.
[6] V. Aravindan, K. Karthikeyan, S. Ravi, S. Amaresh, W.S. Kim, Y.S. Lee, J. Mater. Chem. 20 (2010) 7340–7343.
[7] M. Kuezma, S. Devaraj, P. Balaya, J. Mater. Chem. 22 (2012) 21279–21284.
[8] K. Karthikeyan, V. Aravindan, S.B. Lee, I.C. Jang, H.H. Lim, G.J. Park, M. Yoshio, Y.S. Lee, J. Power Sources 195 (2010) 3761–3764.
[9] Y.-X. Li, Z.-L. Gong, Y. Yang, J. Power Sources 174 (2007) 528–532.
[10] A. Bhaskar, M. Deepa, T.N. Rao, U.V. Varadaraju, J. Electrochem. Soc. 159 (2012) A1954–A1960.
[11] P. Ghosh, S. Mahanty, R.N. Basu, J. Electrochem. Soc. 156 (2009) A677–A681.
[12] R. Dominko, M. Bele, M. Gaberscek, A. Meden, M. Remskar, J. Jamnik, Electrochem. Commun. 8 (2006) 217–222.
[13] M.E. Arroyo-deDompablo, R. Dominko, J.M. Gallardo-Amores, L. Dupont, G. Mali, H. Ehrenberg, J. Jamnik, E. Moran, Chem. Mater. 20 (2008) 5574–5584.

[14] R. Dominko, I. Arcon, A. Kodre, D. Hanzel, M. Gaberscek, J. Power Sources 189 (2009) 51–58.
[15] C. Sirisopanaporn, R. Dominko, C. Masquelier, A.R. Armstrong, G. Mali, P.G. Bruce, J. Mater. Chem. 21 (2011) 17823–17831.
[16] D. Sun, H. Wang, P. Ding, N. Zhou, X. Huang, S. Tan, Y. Tang, J. Power Sources 242 (2013) 865–871.
[17] D. Rangappa, K.D. Murukanahally, T. Tomai, A. Unemoto, I. Honma, Nano Lett. 12 (2012) 1146–1151.
[18] S. Zhang, Y. Li, G. Xu, S. Li, Y. Lu, O. Toprakci, X. Zhang, J. Power Sources 213 (2012) 10–15.
[19] S. Zhang, Z. Lin, L. Ji, Y. Li, G. Xu, L. Xue, S. Li, Y. Lu, O. Toprakci, X. Zhang, J. Mater. Chem. 22 (2012) 14661–14666.
[20] X. Huang, H. Chen, S. Zhou, Y. Chen, J. Yang, Y. Ren, H. Wang, M. Qu, Z. Pan, Z. Yu, Electrochim. Acta 60 (2012) 239–243.
[21] T. Muraliganth, K.R. Stroukoff, A. Manthiram, Chem. Mater. 22 (2010) 5754–5761.
[22] G. Mali, A. Meden, R. Dominko, Chem. Commun. 46 (2010) 3306–3308.
[23] W. Tang, Y.Y. Hou, X.J. Wang, Y. Bai, Y.S. Zhu, H. Sun, Y.B. Yue, Y.P. Wu, K. Zhu, R. Holze, J. Power Sources 197 (2012) 330–333.
[24] J.D. Wilcox, M.M. Doeff, M. Marcinek, R. Kostecki, J. Electrochem. Soc. 154 (2007) A389–A395.
[25] M. Park, X. Zhang, M. Chung, G.B. Less, A.M. Sastry, J. Power Sources 195 (2010) 7904–7929.
[26] H. Wang, K. Huang, Y. Ren, X. Huang, S. Liu, W. Wang, J. Power Sources 196 (2011) 9786–9791.
[27] H. Wang, A. Tang, K. Huang, S. Liu, Trans. Nonferrous Met. Soc. China 20 (2010) 803–808.
[28] F. Nobili, F. Croce, B. Scrosati, R. Marassi, Chem. Mater. 13 (2001) 1642–1646.